DOE/ER/45357--14

FINAL REPORT

Defects and Transport in Mixed Oxides

DOE Grant No. DE-FGO2-88ER45357

(Project Title: Defects and Transport in Mixed Oxides and Kinetics of Solid State Reactions)

DOE Patent Clearance Granted
MP Dvorscak Apr 4, 2002
Mark P Dvorscak Date
(630) 252-2393
E-mail mark.dvorscak@ch.doe.gov
Patent Intellectual Property Law
DOE Chicago Operations Office

Rüdiger Dieckmann
Department of Materials Science and Engineering
Cornell University
Ithaca, NY 14853-1501
(607) 255-4315

December 13, 2001

from CHO 4/11/02

DISCLAIMER

1. INTRODUCTION

The PI of this research program came to Cornell University from Hannover (Germany) in July 1987. The program "*Defects and Transport in Mixed Oxides*" was started in July 1988. When applying for renewals in 1993 and 1996 it was intended to expand the program to include also point defect-related kinetics of solid state reactions and the project title was expanded accordingly. Unfortunately, the final funding levels resulting from both of these renewals were insufficient to expand the program as proposed; therefore the program remained limited to the topics defects and transport in mixed oxides. Between July 2000 and June 2001, the program was continued under a no-cost extension. - The last progress report for this program was written on April 15, 1999 and submitted to DOE with the last continuation proposal.

2. PERSONNEL

Until the end of Spring 2001, one MS student, Mr. HyungSeon Oh, (partially supported from the grant, partially supported as a TA and earlier partially self-supported) and one undergraduate (Ms. Naa-Dei Nikoi) were working for this DOE-supported research program. HyungSeon Oh joined the program in January 1998. In Summer 2001 Mr. Oh left to pursue further graduate studies in Electrical Engineering; his MS thesis is still awaiting completion. Mrs. Li Liu, an MS/PhD student who left in Summer 2000 with a Masters degree was supported from the grant from January 1998 until she left.

3. COLLABORATIONS

During the lifetime of this research program several cooperations were established. The main collaboration was with the group of Professor Klaus-Dieter Becker, Institute for Physical and Theoretical Chemistry, University of Braunschweig, Germany. His principal areas of research and expertise are the high temperature spectroscopy of ionic solids (Mössbauer and optical spectroscopy) and also the transport of matter and charge in ionic solids. For example, Dr. Becker's group was working on the in-situ cation distribution in spinels by performing in-situ spectroscopic measurements at high temperatures. It is worth mentioning that the collaboration with Dr. Becker's group was intensified since 1996 with the help of a NATO travel grant awarded to us in December 1995 and extended later until the end of 1999.

4. PERFORMED RESEARCH

In the following, mainly results obtained after the progress report of April 15, 1999 are reported. Significant progress has since then been made in the areas of: (i) the non-stoichiometry and the cation tracer diffusion in oxide solid solutions of the type $(Fe,Me)_{3-\delta}O_4$, (ii) the grain size dependence of the variation of the oxygen content in $Cu_{2-\delta}O$, (iii) and the influence of the cationic composition of $La_{1-x}Mn_{1+x}O_{3-\delta}$ on δ and on the point defect relaxation in this material.

4.1. Nonstoichiometry and Cation Tracer Diffusion in Oxide Solid Solutions of the Type $(Me_xFe_{1-x})_{3-\delta}O_4$

In 1999 and in the first part of 2000 the graduate student Li Liu (supported from the grant) has continued and completed her experimental work on the variation of the oxygen content and the cation tracer diffusion in $(Ni_xFe_{1-x})_{3-\delta}O_4$ as a function of the cationic composition, x, and the oxygen activity, a_{O_2}, at 1200 °C. She has also performed some experimental work on the variation of the oxygen content in iron based spinels where Me consists partially of Mn and partially of Zn, i.e., on spinels of the type $Zn_xMn_{1-x-y}Fe_{2+y}O_4$. Li Liu has summarized the results of her work in a Master's thesis before leaving Cornell in Summer 2000. Two publications are in preparation.

Figs. 1-4 (see next page) show the variation of δ in $(Ni_xFe_{1-x})_{3-\delta}O_4$ with x = 0.0, 0.1, 0.25, and 0.30 at 1200 °C, respectively, with the oxygen activity, a_{O_2} (= P_{O_2}/P°; P° = 1 atm). In all cases S-shape δ vs. log a_{O_2} curves were found. At high oxygen activities, these curves are bent upwards, indicating that cation vacancies are the majority point defects. At low oxygen activities, the δ vs. log a_{O_2} curves are bent downwards; this indicates that cation interstitials are here the majority defects. All curves shown in Figs. 1-4 were drawn by fitting the experimental data to a point defect model. δ as a function of log a_{O_2} follows the equation

$$\delta = [V]^\circ \cdot a_{O_2}^{2/3} - [I]^\circ \cdot a_{O_2}^{-2/3} \qquad (1)$$

where $[V]^\circ$ and $[I]^\circ$ represent point defect concentrations normalized to $a_{O_2} = 1$. $[V]^\circ$ and $[I]^\circ$ are called defect constants of cation vacancies and of cation interstitials, respectively. All δ vs. log a_{O_2} curves show an inflection point at $\delta = 0$. Here the concentrations of cation vacancies and of cation interstitials are equal and the spinel is stoichiometric.

To measure tracer diffusion coefficients of Fe and Ni, we used the radioactive tracers Fe-59 and Ni-63. When decaying, Fe-59 emits both γ- and β-radiation, while Ni-63 emits only β-radiation. The energy of the γ-rays emitted by Fe-59 is sufficiently high so that the absorption of the emitted radiation within the samples studied can be ignored for the geometries used in the experiments. However, the absorption of the β-rays emitted by Fe-59 and Ni-63 in the sample material must be properly taken into account when evaluating experimental data because these ß-rays have relatively low energies and are therefore strongly absorbed.

For evaluating tracer diffusion profiles we have in all cases measured residual radioactivities, i.e., the amounts of radioactivity left in a sample after the removal of material of different thickness. Tracer diffusion coefficients were calculated from residual radioactivity profiles by using the proper solution of Fick's second law, taking the absorption properly

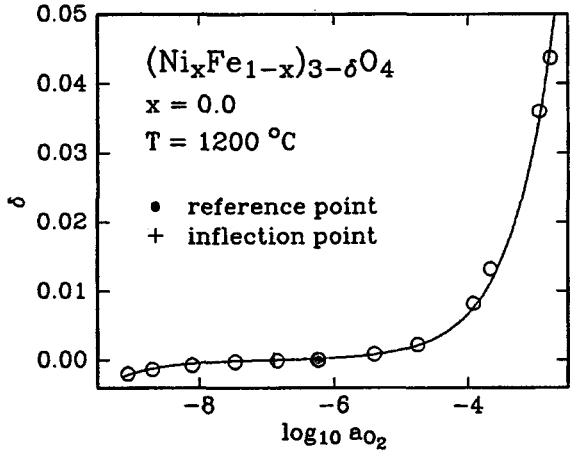

Fig. 1: Deviation from stoichiometry, δ, in $(Ni_xFe_{1-x})_{3-\delta}O_4$ with x = 0.0 at 1200 °C as a function of the oxygen activity, a_{O_2}.

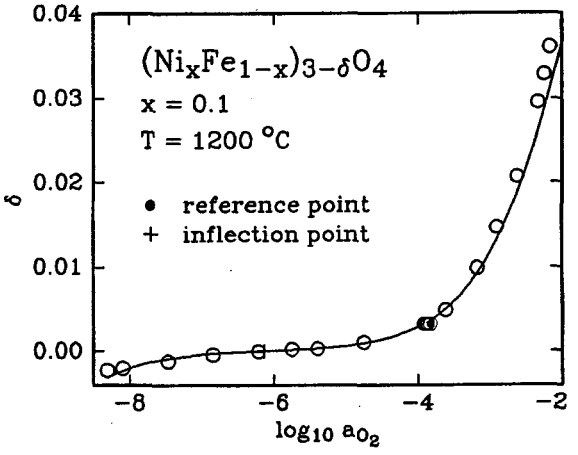

Fig. 2: Deviation from stoichiometry, δ, in $(Ni_xFe_{1-x})_{3-\delta}O_4$ with x = 0.1 at 1200 °C as a function of the oxygen activity, a_{O_2}.

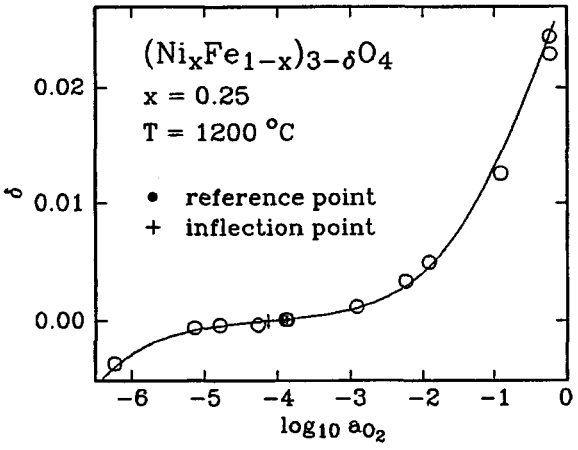

Fig. 3: Deviation from stoichiometry, δ, in $(Ni_xFe_{1-x})_{3-\delta}O_4$ with x = 0.25 at 1200 °C as a function of the oxygen activity, a_{O_2}.

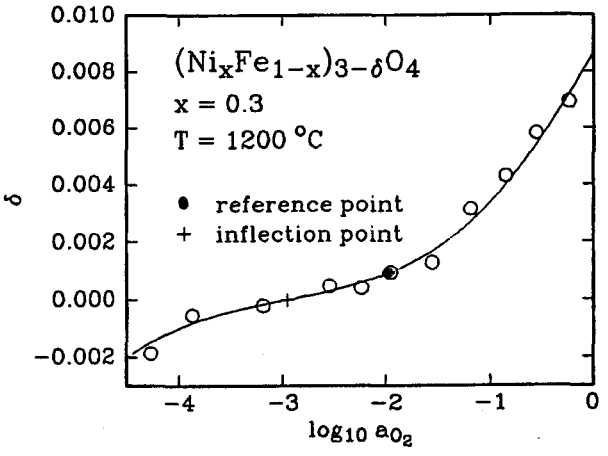

Fig. 4: Deviation from stoichiometry, δ, in $(Ni_xFe_{1-x})_{3-\delta}O_4$ with x = 0.30 at 1200 °C as a function of the oxygen activity, a_{O_2}.

into account in the cases of ß-radiation emitted from Fe-59 or from Ni-63, see Eq. 2, or ignoring the absorption in the case of the γ-radiation of Fe-59, see Eq. 3.

$$\frac{A(\xi,t)}{A(0,t)} = \exp\left(\mu_{Me}\cdot\xi\right)\cdot\frac{1-\operatorname{erf}\left(\dfrac{\xi}{2\cdot\sqrt{D^*_{Me}\cdot t}}+\mu_{Me}\cdot\sqrt{D^*_{Me}\cdot t}\right)}{1-\operatorname{erf}\left(\mu_{Me}\cdot\sqrt{D^*_{Me}\cdot t}\right)} \qquad (2)$$

μ_{Me} is the absorption coefficient of the sample material for the isotope considered.

$$\frac{A(\xi,t)}{A(0,t)} = 1-\operatorname{erf}\left(\frac{\xi}{2\cdot\sqrt{D^*_{Me}\cdot t}}\right) \qquad (3)$$

Fig. 5 shows a comparison of β- and γ-radiation residual activity profiles for Fe-59 for a selected diffusion experiment. This figure clearly shows that the profiles obtained are significantly different from each other. However, properly taking into account the absorption in the case of the ß-radiation leads to practically identical tracer diffusion coefficients.

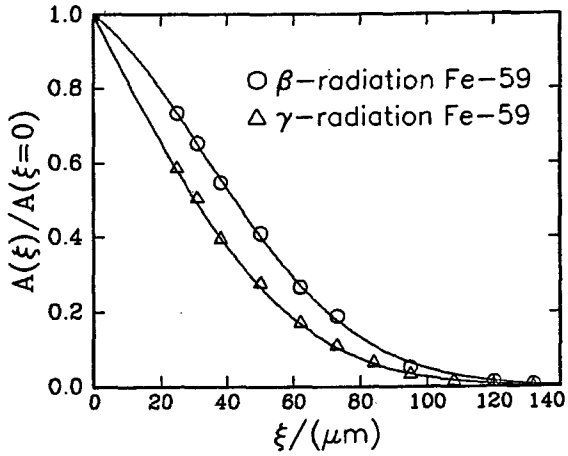

Fig. 5: Comparison of ß-and γ-residual activity profiles for a diffusion experiment performed with Fe-59.

Fig. 6 shows a residual activity profile for the diffusion of Ni-63 in $(Ni_xFe_{1-x})_{3-\delta}O_4$ with $x = 0.25$ at 1200 °C and log $a_{O_2} = -3.80$. For the diffusion of Fe-59, due to the relatively high energy of the γ-radiation, the absorption can be ignored. The iron tracer diffusion coefficients were obtained by a linear least squares fit to a penetration profile in the form of the inverse of the error function of $1 - A(\xi)/A(\xi=0)$ (where $A(\xi)$ is the residual activity after the removal of a layer with the thickness ξ and $A(\xi=0)$ is the residual activity before any material removal); Fig. 7 shows such a profile.

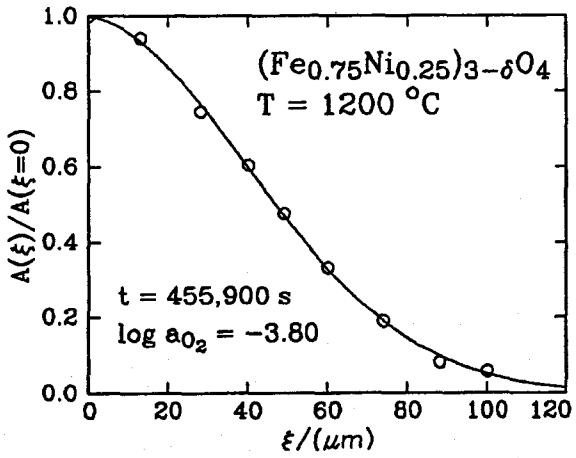

Fig. 6: Residual activity profile for Ni-63 diffused for 455,900 s into $(Ni_{0.25}Fe_{0.75})_{3-\delta}O_4$ at 1200 °C and log $a_{O_2} = -3.8$.

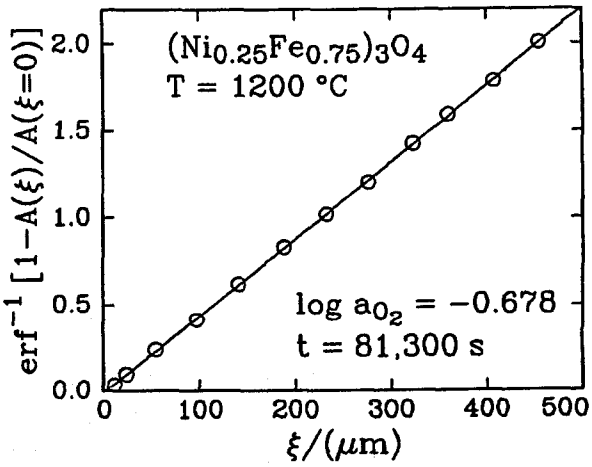

Fig. 7: Penetration profile for Fe-59 diffused for 81,300 s into $(Ni_{0.25}Fe_{0.75})_{3-\delta}O_4$ at 1200 °C and log $a_{O_2} = -0.678$.

After the submission of the last project report many new diffusion data have been measured. Figs. 8-11 (see next page) show the variation of cation tracer diffusion coefficients of Ni and Fe with the oxygen activity at 1200 °C in $(Ni_xFe_{1-x})_{3-\delta}O_4$ with $x =$ 0.10, 0.20, 0.25, and 0.30, respectively. The data denoted in Figs. 10 and 11 by "Fe^{59} Longhi" have been measured by a former member of our group who left before Li

Liu joined the group. V-shaped curves were found for all log D^*_{Me} vs. log a_{O_2} for Me = Ni and Fe. The observed oxygen activity dependences can be described by equations of the type

$$D^*_{Me} = D^*_{Me[V]} \cdot a_{O_2}^{2/3} + D^*_{Me[I]} \cdot a_{O_2}^{-2/3} \qquad (4)$$

$D^*_{Me[V]}$ and $D^*_{Me[I]}$ represent partial tracer diffusion coefficients of the metal Me diffusing via vacancies and via interstitials, respectively, both normalized to $a_{O_2} = 1$. The oxygen activity dependences observed for the tracer diffusion coefficients indicate that at high oxygen activities the cation diffusion is governed by cation vacancies and by cation interstitials at low oxygen activities.

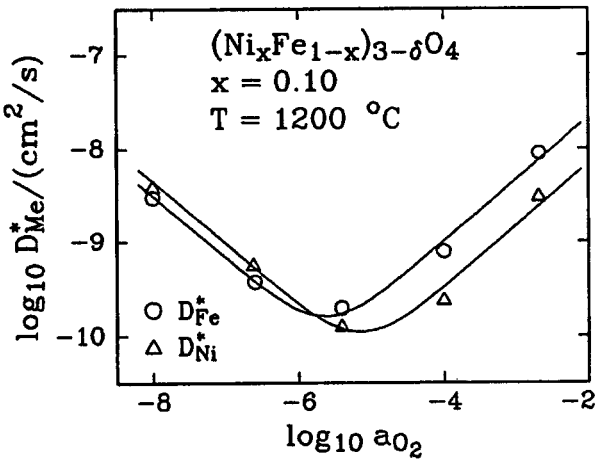

Fig. 8: Oxygen activity dependence of D^*_{Fe} and D^*_{Ni} in $(Ni_xFe_{1-x})_{3-\delta}O_4$ with x = 0.1 at 1200 °C.

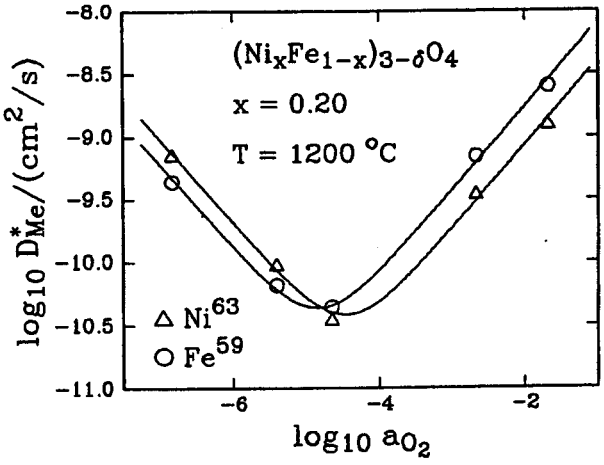

Fig. 9: Oxygen activity dependence of D^*_{Fe} and D^*_{Ni} in $(Ni_xFe_{1-x})_{3-\delta}O_4$ with x = 0.2 at 1200 °C.

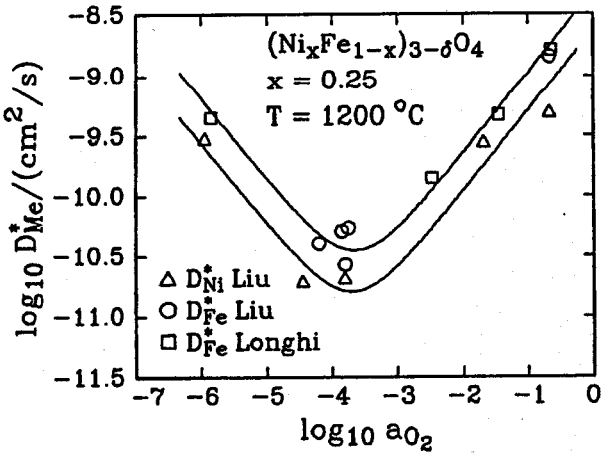

Fig. 10: Oxygen activity dependence of D^*_{Fe} and D^*_{Ni} in $(Ni_xFe_{1-x})_{3-\delta}O_4$ with x = 0.25 at 1200 °C.

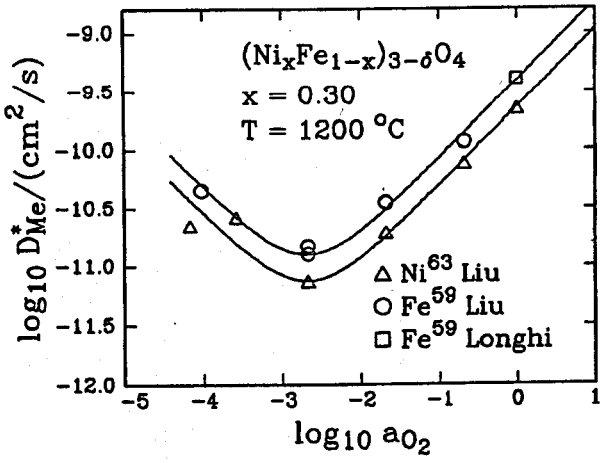

Fig. 11: Oxygen activity dependence of D^*_{Fe} and D^*_{Ni} in $(Ni_xFe_{1-x})_{3-\delta}O_4$ with x = 0.3 at 1200 °C.

Fig. 12 gives a summary of the tracer diffusion data measured for Ni-63 and Fe-59 diffusing in $(Ni_xFe_{1-x})_{3-\delta}O_4$. At high oxygen activities, the difference between D^*_{Fe} and D^*_{Ni} increases with a decreasing Ni concentration. At low oxygen activities, D^*_{Ni} becomes closer to D^*_{Fe} with increasing x and at larger values of x finally becomes larger than D^*_{Fe}. This behavior is most likely related to changes in the cation and/or defect distribution with the cationic composition x.

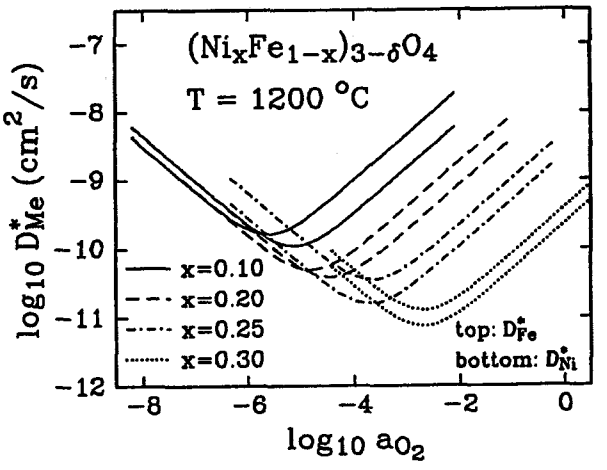

Fig. 12: Summary of the iron and nickel tracer diffusion data measured in this study in $(Ni_xFe_{1-x})_{3-\delta}O_4$ at 1200 °C.

Solid solutions of the type $(Me_xFe_{1-x})_{3-\delta}O_4$ with Me = Co are expected to behave similar to the nickel analogue because of the similarity between Co^{2+} and Ni^{2+} ions. Figs. 13 and 14 show the data obtained for the normalized tracer diffusivities $D^*_{Me[V]}$ and Figs. 15 and 16 (see next page) $D^*_{Me[I]}$ for $(Ni_xFe_{1-x})_{3-\delta}O_4$ and for $(Co_xFe_{1-x})_{3-\delta}O_4$ (from earlier work in this program [1]), respectively. There is a very similar behavior of $D^*_{Me[V]}$ in both types of spinels; $D^*_{Me[V]}$ decreases with an increasing degree of substitution of iron ions. However, $D^*_{Ni[V]} < D^*_{Fe[V]}$ in $(Ni_xFe_{1-x})_{3-\delta}O_4$ solid solutions while $D^*_{Co[V]} \approx D^*_{Fe[V]}$ in $(Co_xFe_{1-x})_{3-\delta}O_4$ solid solutions. A comparison between Figs. 15 and 16 yields that $D^*_{Me[I]}$ increases in both solid solutions considered here with an increasing degree of substitution of iron ions through Ni or Co ions. At a low content of Me one finds in both types of spinels $D^*_{Me[I]} > D^*_{Fe[I]}$. However, in the case of $(Ni_xFe_{1-x})_{3-\delta}O_4$ solid solutions this relation changes to $D^*_{Ni[I]} < D^*_{Fe[I]}$ at a high content of Ni. This behavior may be related to differences in the distribution of interstitial ions on differently coordinated interstitial positions.

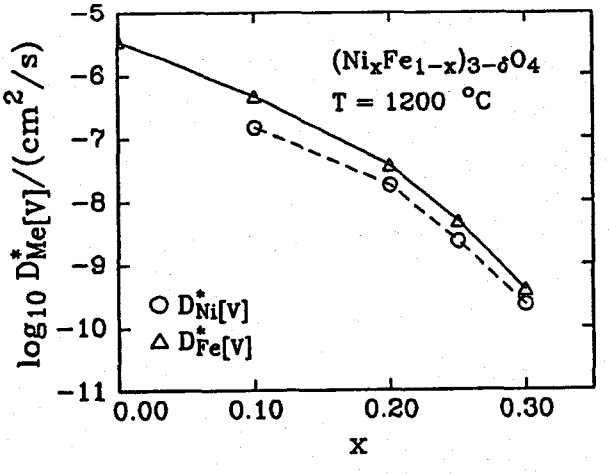

Fig. 13: Normalized tracer diffusion coefficients of cations diffusing in $(Ni_xFe_{1-x})_{3-\delta}O_4$ at 1200 °C via cation vacancies as a function of x.

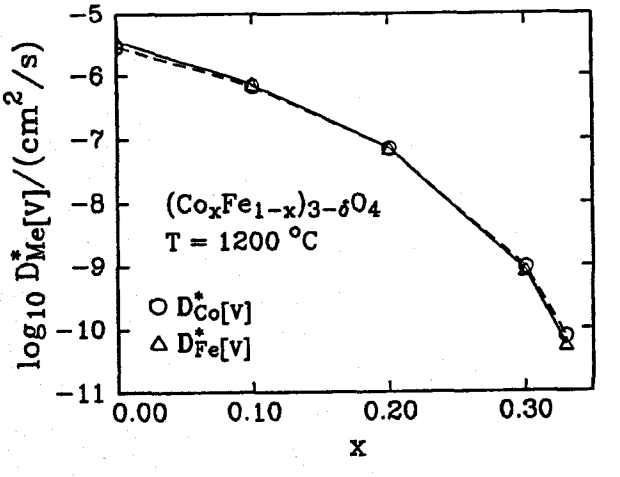

Fig. 14: Normalized tracer diffusion coefficients of cations diffusing in $(Co_xFe_{1-x})_{3-\delta}O_4$ at 1200 °C via cation vacancies as a function of x.

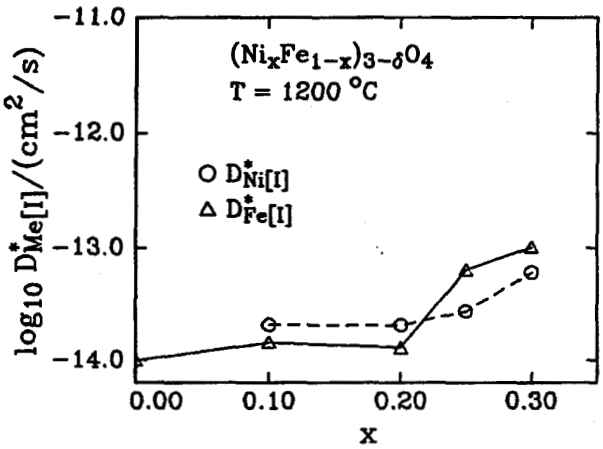

Fig. 15: Normalized tracer diffusion coefficients of cations diffusing in $(Ni_xFe_{1-x})_{3-\delta}O_4$ at 1200 °C via cation interstitials as a function of x.

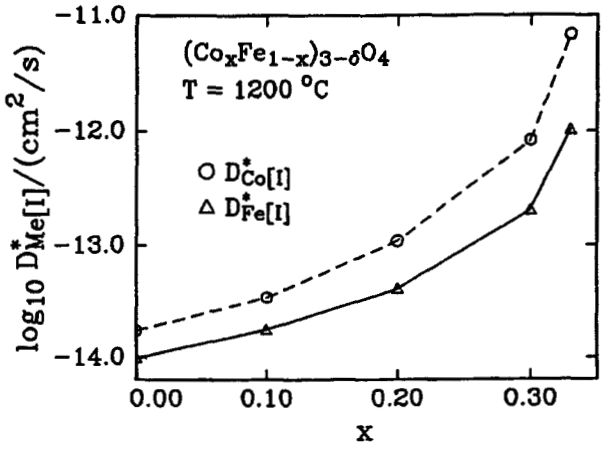

Fig. 16: Normalized tracer diffusion coefficients of cations diffusing in $(Co_xFe_{1-x})_{3-\delta}O_4$ at 1200 °C via cation interstitials as a function of x.

We also performed some measurements on the deviation from stoichiometry as a function of a_{O_2} at 1200 °C in spinels of the type $Zn_xMn_{1-x-y}Fe_{2+y}O_4$. Ferrites of this type have wide applications in the electronic industry. The results of our measurements are summarized in the δ vs. log a_{O_2} plots shows in Figs. 17-22. In Figs. 17-21 y = 0 and in Fig. 22 y = 0.081. The composition considered in Fig. 22 is often used in commercial ferrites. All data shown in Figs. 17-22 were measured by Li Liu, except about half of the data shown in Fig. 22; the latter data points were measured by a former post-doc in our group, Jörg Töpfer, when re-visiting our laboratory in Summer 1999. All curves shown in Figs. 17-22 at 1200 °C are S-shaped. From the observed oxygen activity dependences we conclude

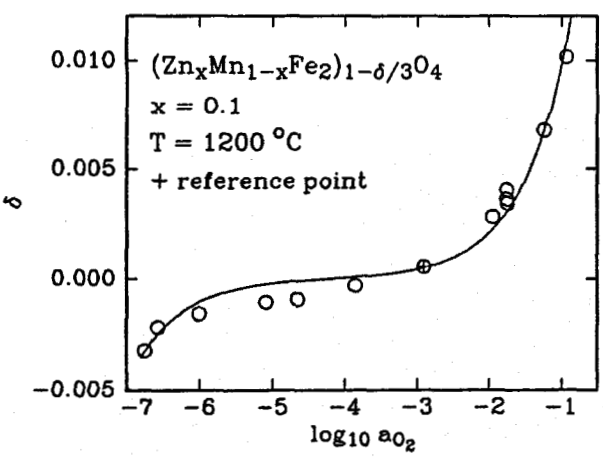

Fig. 17: Deviation from stoichiometry, δ, in $(Zn_xMn_{1-x-y}Fe_{2+y})_{1-\delta/3}O_4$ with x = 0.1 and y = 0 at 1200 °C as a function of log a_{O_2}.

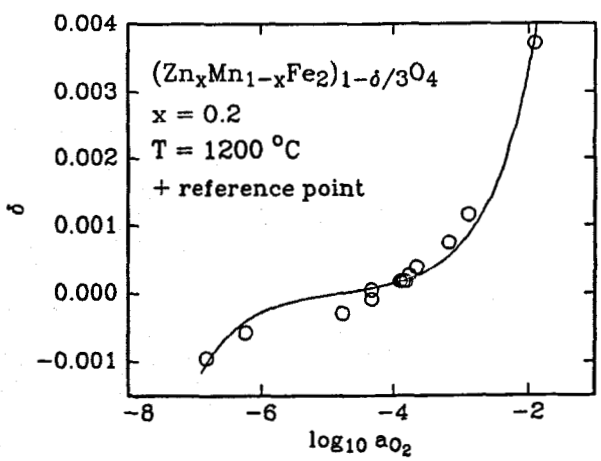

Fig. 18: Deviation from stoichiometry, δ, in $(Zn_xMn_{1-x-y}Fe_{2+y})_{1-\delta/3}O_4$ with x = 0.2 and y = 0 at 1200 °C as a function of log a_{O_2}.

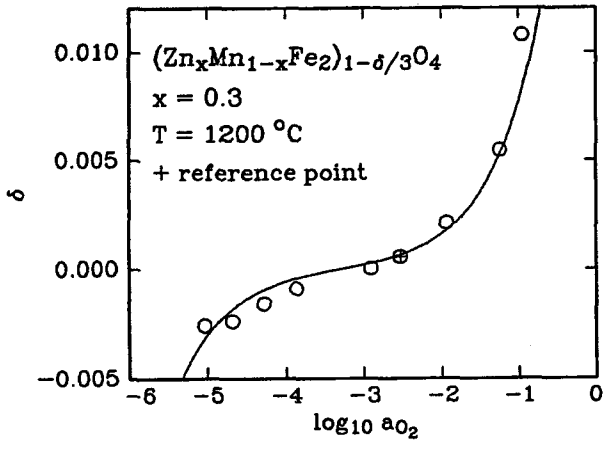

Fig. 19: Deviation from stoichiometry, δ, in $(Zn_xMn_{1-x-y}Fe_{2+y})_{1-\delta/3}O_4$ with x = 0.3 and y = 0 at 1200 °C as a function of log a_{O_2}.

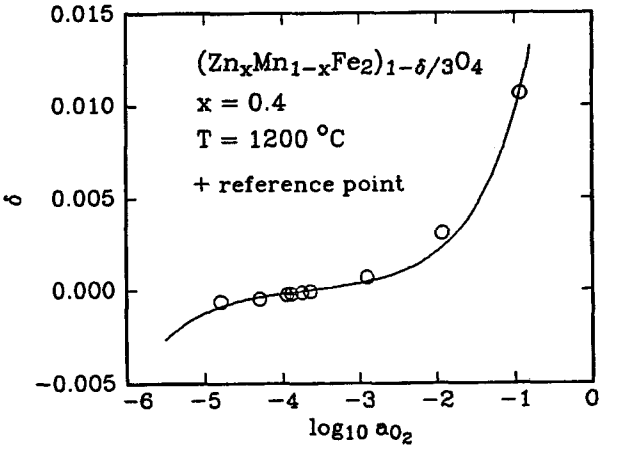

Fig. 20: Deviation from stoichiometry, δ, in $(Zn_xMn_{1-x-y}Fe_{2+y})_{1-\delta/3}O_4$ with x = 0.4 and y = 0 at 1200 °C as a function of log a_{O_2}.

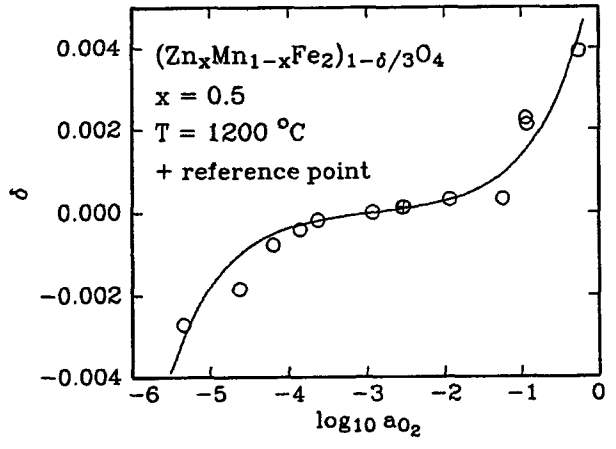

Fig. 21: Deviation from stoichiometry, δ, in $(Zn_xMn_{1-x-y}Fe_{2+y})_{1-\delta/3}O_4$ with x = 0.5 and y = 0 at 1200 °C as a function of log a_{O_2}.

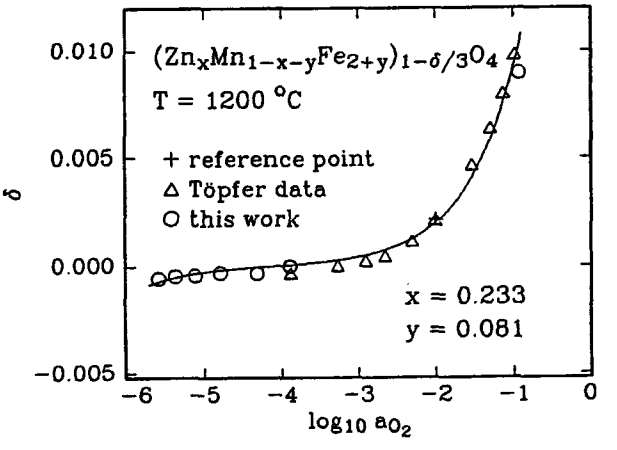

Fig. 22: Deviation from stoichiometry, δ, in $(Zn_xMn_{1-x-y}Fe_{2+y})_{1-\delta/3}O_4$ with x = 0.1 and y = 0.081 at 1200 °C as a function of log a_{O_2}.

that in all manganese zinc ferrites investigated cation vacancies are the majority defects at high oxygen activities while cation interstitials are the majority defects at low oxygen activities. The curves shown in the figures have been obtained by fitting the experimental data to Eq. (1). The values obtained for the defect constants [V]° and [I]° from the data fitting are shown in Figs. 23 and 24 (see next page). Although the data scatter to some extent it follows from Figs. 23 and 24 that the zinc concentration has a strong influence on the values of the defect constants. It becomes more difficult to make cation vacancies when Mn is replaced by Zn while it becomes at the same time easier to create cation interstitials. The detailed reasons for this phenomena are not yet clear.

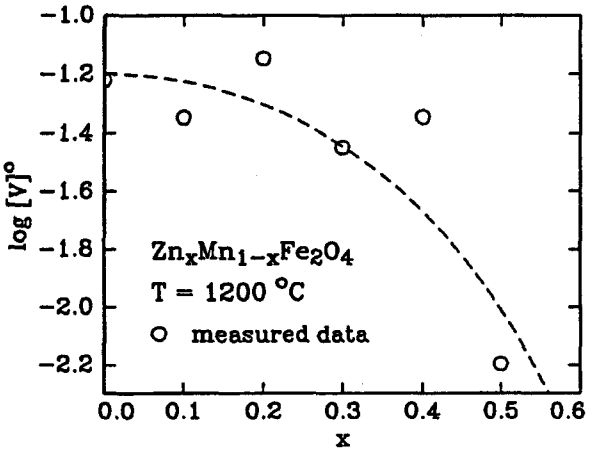

Fig. 23: Variation of the defect constant for the formation of cation vacancies as a function of the zinc concentration, x.

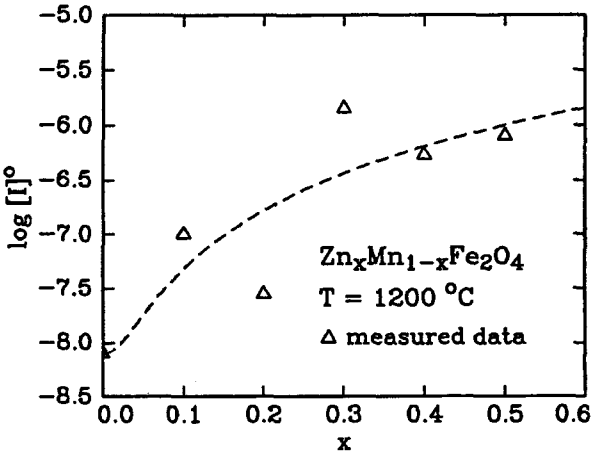

Fig. 24: Variation of the defect constant for the formation of cation interstitials as a function of the zinc concentration, x.

4.2. Grain Size Dependence of the Variation of the Oxygen Content In Cuprous Oxide, $Cu_{2-\delta}O$

As discussed in a previous report, we had performed some experimental work on the influence of near-boundary regions on the non-stoichiometry of cuprous oxide. Experimental results for 800 °C are shown in Fig. 25. Similar results were obtained for 750 and 900 °C. We found that in fine-grained $Cu_{2-\delta}O$ the relative change in the deviation from stoichiometry, $\Delta\delta$, was larger than in coarse-grained $Cu_{2-\delta}O$ and that the grain size had a significant influence on δ even in relatively large-grained samples. We had discussed different approaches to model the observed variation in the deviation from stoichiometry with grain size.

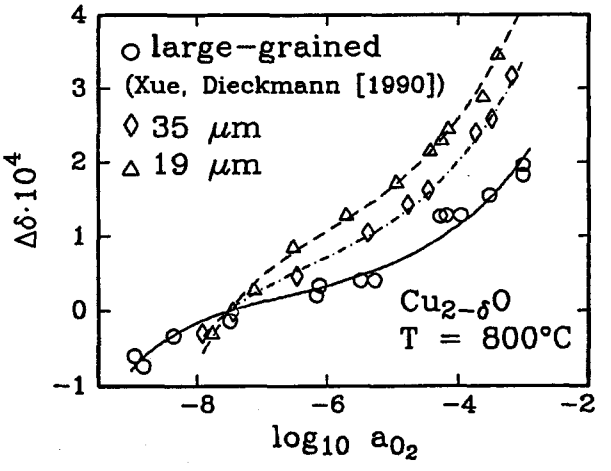

Fig. 25: Variation of the oxygen content of polycrystalline $Cu_{2-\delta}O$ with different grain size as a function of log a_{O_2} at 800 °C.

In order to narrow further down the possibilities to interpret the experimental results, an undergraduate student (Naa-Dei Nikoi) tried to prepare more fine-grained $Cu_{2-\delta}O$ by chemical synthesis. She succeeded to produce powders with particle sizes of around one micrometer and below. Hot-pressing of such powders to solid samples for electrical conductivity measurements followed. If space charges are involved in the changes discussed above there should be a strong variation of the electrical conductivity with the grain size. Such a variation was not observed, suggesting that the presence of space

charges is unlikely to be responsible for the observed grain size dependence of the variation of δ with oxygen activity.

4.3. Influence of the Cationic Composition of $La_{1-x}Mn_{1+x}O_{3+\delta}$ on δ and on the Kinetics of the Point Defect Relaxation

Lanthanum manganate, "$LaMnO_3$," is the base material of the cathodes used nowadays in solid oxide fuel cells. Such cathodes are usually made from SrO-doped "$LaMnO_3$." Sometimes, for cost and other reasons, some of the La is replaced by other cations. To better understand the behavior of $LaMnO_3$-based solid oxide fuel cell cathode materials we have initiated a study on the influence of the cationic composition and of the oxygen activity on the variation of the oxygen content and also on the kinetics of the point defect relaxation, beginning with undoped $LaMnO_3$.

$LaMnO_3$ is a non-stoichiometric perovskite in which the oxygen content and the cation composition can be varied to some extent. Therefore, if one wants to be more precise, it is more appropriate to use the notation "$La_{1-x}Mn_{1+x}O_{3+\delta}$" for lanthanum manganite than using just "$LaMnO_3$." Van Roosmalen et al. [2] have published a phase diagram for the system La-Mn-O which is shown in Fig. 26. According to this diagram the cationic composition, i.e., the value of x, can be varied at high temperatures to a very significant extent within the stability range of lanthanum manganite. In addition, the cation-to-anion ratio, i.e., the deviation from stoichiometry, δ, can be varied very significantly with the oxygen activity. In principle, one must expect that the stability range of lanthanum manganite varies not only with the temperature but simultaneously also with other intensive variables, e.g., with the oxygen activity. However, in the literature we did not find any systematic data on the variation of x with the oxygen activity in lanthanum manganite in equilibrium with La_2O_3 or with manganese oxide. This subject is worth to be looked at in the future.

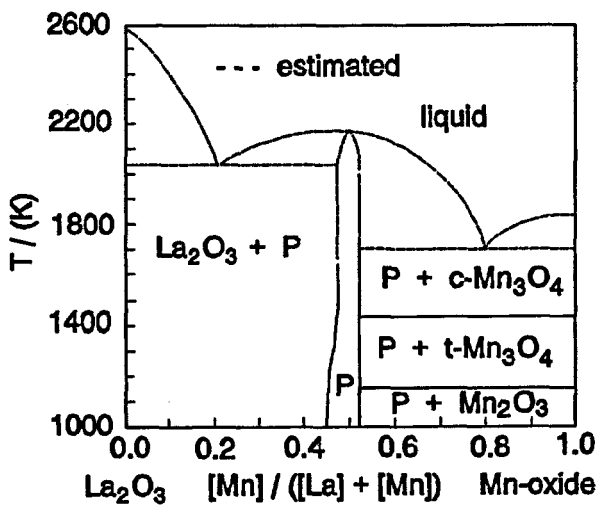

Fig. 26: La_2O_3-Mn-oxide phase diagram [2].

Important properties of interest for a solid oxide fuel cell cathode material are it's ionic and electronic conductivities, it's chemical reactivity with other solid oxide fuel cell components (electrolyte, interconnect), and also it's reactivity with oxygen-containing gases. A high rate for the incorporation of oxygen into the cathode material is very critical

for reducing the polarization at the cathode. All important properties just mentioned are (in different ways) related to the point defect structure of the cathode material. To further improve currently existing cathode materials and to look for better other perovskite-based cathode materials it is very important to better understand the underlying point defect chemistry of perovskites in general and of lanthanum manganite in detail. Our approach to contribute to this area was to study this subject first in undoped, very clean lanthanum manganite with the intent to look later systematically at the influence of dopants, departing from pure lanthanum manganite, and finally to extend our work to other non-stoichiometric perovskites. This will be the subject of a new research program.

In the following we will focus on undoped lanthanum manganite, the main topic of the research of HyungSeon Oh, a former graduate student. We were not the first group trying to improve the limited understanding of point defects in lanthanum manganite. Measurements of the deviation from stoichiometry, δ, and of the electrical conductivity, σ, have been performed by several groups, see, e.g., Refs. [3]-[6]. For the deviation from stoichiometry, S-shaped curves have been measured for δ as a function of log a_{O_2}. Some experimental results for the variation of δ in $LaMnO_{3+\delta}$ at 1100 °C are shown in Fig. 27. At low and at high oxygen activities δ changes rapidly with the oxygen activity while there are only small changes at intermediate oxygen activities. At low a_{O_2} anion vacancies and electrons are the predominant defect species while holes and cation vacancies predominate at high a_{O_2}. It is relatively unclear how the cation vacancies are distributed between the different types of cation sites (A(=La)- and B(=Mn)-sites). In addition, it is also not clear how the cations are exactly distributed between A and B sites, even when x = 0. Data for the electrical conductivity, σ, also at 1100 °C, are shown in Fig. 28. The data available for σ and also thermopower data from the litera-

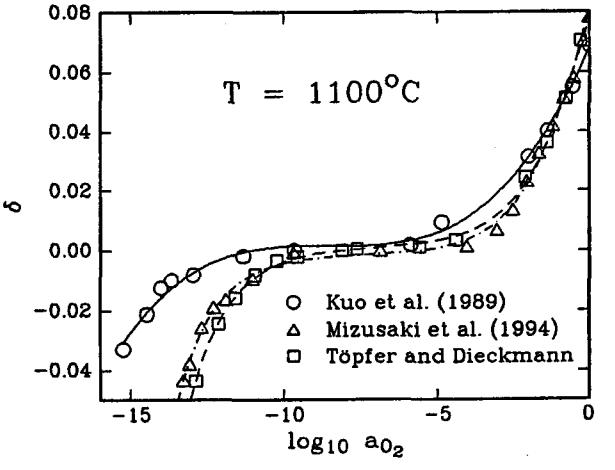

Fig. 27: Deviation from stoichiometry, δ, in $LaMnO_{3+\delta}$ at 1100 °C as a function of the oxygen activity, a_{O_2}.

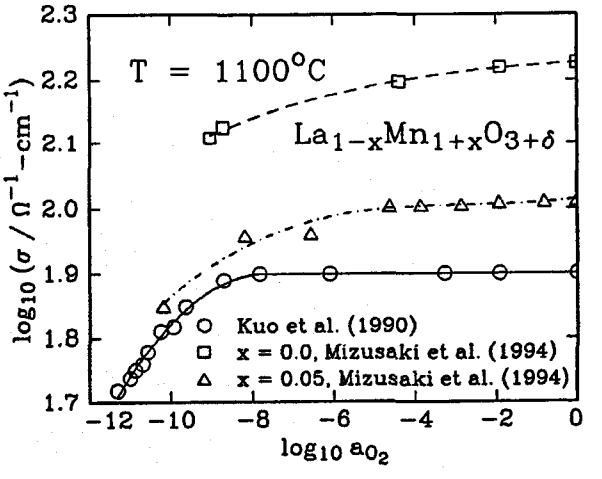

Fig. 28: Electrical conductivity, σ, in $LaMnO_{3+\delta}$ at 1100 °C as a function of the oxygen activity, a_{O_2}.

ture suggest that the electrical conduction in lanthanum manganite is p-type at all oxygen activities although electrons are the predominant electronic point defects at low a_{O_2}. Furthermore, the electrical conductivity, σ, is approximately constant at high a_{O_2} even though the overall hole concentration here strongly increases with the oxygen activity. All explanations offered so far for the behavior of σ as a function of a_{O_2} have some shortcomings and are in several cases inconsistent with some experimental observations.

As stated above, the deviation from stoichiometry, δ, and the electrical conductivity, σ, are both closely related to point defect concentrations. Kröger-Vink diagrams are very useful tools to show how different point defect concentrations vary as a function of the oxygen activity. Most of such diagrams published so far for perovskites were derived by making very limiting assumptions, e.g., for the location of different species, unfortunately, often without sufficient justification. To become able to produce Kröger-Vink diagrams for perovskites like $La_{1-x}Mn_{1+x}O_{3+\delta}$ at thermodynamic equilibrium, we have initiated work on the point defect thermodynamics of perovskites by using only a very few assumptions, much less than usually made. In the work performed, we made only three assumptions: (i) interstitial ions do not occur in any significant concentrations, (ii) A ions occur only in the form of 3+ ions, and (iii) there is no significant associate or cluster formation at the point defect concentrations of interest for our modeling. The first assumption is justified by the densely packed structures of perovskites, the second assumption by the very large energy changes associated with valence state changes of La^{3+} and similar (= A^{3+}) ions, and the third assumption by the fact that in-situ neutron scattering experiments (on other oxides) have not shown any hints on very significant associate and cluster formation at high temperatures and in the defect concentration range of interest here.

In our Kröger-Vink diagram calculations for a model perovskite of the type $A_{1-x}B_{1+x}O_{3+\delta}$ we have considered 9 different defect species, vacancies on three sublattices, $(V_O 2-)^{\bullet\bullet}$, $(V_A 3+)'''$, $(V_B 3+)'''$, misplaced cations, $(A^{3+}_{B} 3+)^x$, $(B^{3+}_{A} 3+)^x$, and differently localized charge carriers, $(B^{2+}_{A} 3+)'$, $(B^{4+}_{A} 3+)^{\bullet}$, $(B^{2+}_{B} 3+)'$, $(B^{4+}_{B} 3+)^{\bullet}$. In addition, there are four other concentrations/quantities of importance: δ, $(A^{3+}_{A} 3+)^x$, $(B^{3+}_{B} 3+)^x$, and $(O^{2-}_{O} 2-)^x$. Therefore, thirteen independent equations are required for relating unequivocally δ and the concentrations of all species listed above. Seven equilibrium constants, K_{e1}, K_{e2}, K_{e3}, K_S, K_O, K_A and K_B, can be introduced for defect formation reactions. K_{e1}, K_{e2}, K_{e3} are equilibrium constants for redox reactions occurring on different sublattices:

$$2\,(B^{3+}_{B^{3+}})^x \rightleftharpoons (B^{2+}_{B^{3+}})' + (B^{4+}_{B^{3+}})^{\bullet} \quad K_{e1} \tag{5}$$

$$(B^{3+}_{A^{3+}})^x + (B^{3+}_{B^{3+}})^x \rightleftharpoons (B^{2+}_{B^{3+}})' + (B^{4+}_{A^{3+}})^{\bullet} \quad K_{e2} \tag{6}$$

$$(B^{3+}_{A^{3+}})^x + (B^{2+}_{B^{3+}})' \rightleftharpoons (B^{2+}_{A^{3+}})' + (B^{3+}_{A^{3+}})^x \quad K_{e3} \tag{7}$$

K_S is the equilibrium constant for the Schottky disorder reaction

$$(A_{A^{3+}}^{3+})^x + (B_{B^{3+}}^{3+})^x + 3(O_{O^{2-}}^{2-})^x \rightleftharpoons (V_{A^{3+}})''' + (V_{B^{3+}})''' + 3(V_{O^{2-}})^{\bullet\bullet} + ABO_3(srg) \quad K_S \tag{8}$$

K_O is the equilibrium constant for the component activity dependent reaction

$$2(B_{B^{3+}}^{3+})^x + (O_{O^{2-}}^{2-})^x \rightleftharpoons (V_{O^{2-}})^{\bullet\bullet} + 2(B_{B^{3+}}^{2+})' + \frac{1}{2}O_2(g) \quad K_O \tag{9}$$

Finally, K_A, K_B are equilibrium constants for reactions involving the removal of a molecule of ABO_3 from one cation sublattice and allowing for a cation exchange:

$$(X_{X^{3+}}^{3+})^x + (Y_{X^{3+}}^{3+})^x + 3(O_{O^{2-}}^{2-})^x \rightleftharpoons 2(V_{X^{3+}})''' + 3(V_{O^{2-}})^{\bullet\bullet} + ABO_3(srg) \quad K_i \tag{10}$$

For the A sublattice, X = A, Y = B, and $K_i = K_A$, and for the B sublattice Y = A, X = B, and $K_i = K_B$.

The electroneutrality condition involving all species carrying excess charges is

$$3[(V_{A^{3+}})'''] + 3[(V_{B^{3+}})'''] + [(B_{A^{3+}}^{2+})'] + [(B_{B^{3+}}^{2+})'] = 2[(V_{O^{2-}})^{\bullet\bullet}] + [(B_{A^{3+}}^{4+})^{\bullet}] + [(B_{B^{3+}}^{4+})^{\bullet}] \tag{11}$$

In addition, the two following cation-to-anion balances hold for $A_{1-x}B_{1+x}O_{3+\delta}$:

$$\frac{n_A}{n_O} = \frac{[(A_{A^{3+}}^{3+})^x] + [(A_{B^{3+}}^{3+})^x]}{[(O_{O^{2-}}^{2-})^x]} = \frac{1 - x}{3 + \delta} \tag{12}$$

$$\frac{n_B}{n_O} = \frac{[(B_{A^{3+}}^{2+})] + [(B_{A^{3+}}^{3+})] + [(B_{A^{3+}}^{4+})] + [(B_{B^{3+}}^{2+})] + [(B_{B^{3+}}^{3+})] + [(B_{B^{3+}}^{4+})]}{[(O_{O^{2-}}^{2-})^x]} = \frac{1 + x}{3 + \delta} \tag{13}$$

Because a perovskite of the type $A_{1-x}B_{1+x}O_{3+\delta}$ has three different sublattices, three different site balances must be fulfilled. These site balances are:

$$[(A_{A^{3+}}^{3+})^x] + [(B_{A^{3+}}^{2+})'] + [(B_{A^{3+}}^{3+})^x] + [(B_{A^{3+}}^{4+})^{\bullet}] + [(V_{A^{3+}})'''] = 1 \tag{14}$$

$$[(B_{B^{3+}}^{2+})'] + [(B_{B^{3+}}^{3+})^x] + [(B_{B^{3+}}^{4+})^{\bullet}] + [(A_{B^{3+}}^{3+})^x] + [(V_{B^{3+}})'''] = 1 \tag{15}$$

and

$$[(O_{O^{2-}}^{2-})^x] + [(V_{O^{2-}})^{\bullet\bullet}] = 3 \tag{16}$$

For demonstration purposes we have calculated Kröger-Vink diagrams by using one set of arbitrarily selected equilibrium constants for all values of x and assuming an ideal solution of point defects. One set of diagrams obtained by using the same set of constants but different values for the composition parameter x are shown in Figs. 29, 30 and 31.

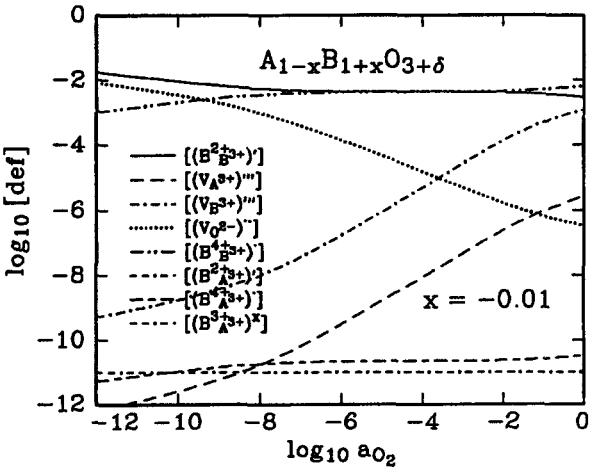

Fig. 29: Kröger-Vink diagram for $A_{1-x}B_{1+x}O_{3+\delta}$ with x = −0.01.

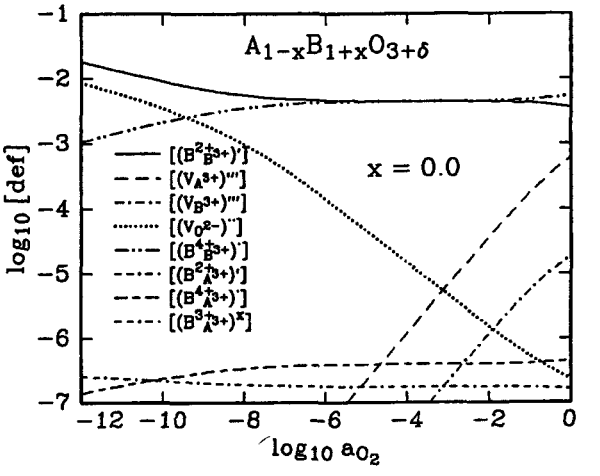

Fig. 30: Kröger-Vink diagram for $A_{1-x}B_{1+x}O_{3+\delta}$ with x = 0.00.

In the diagrams shown in Figs. 29-31 the majority defects at low a_{O_2} are $(V_O{}^{2-})^{\bullet\bullet}$ and $(B^{2+}_{Me}{}^{3+})'$ (= electrons localized at B^{3+} ions on the Me sublattice), and at high a_{O_2} $(V_{Me}{}^{3+})'''$ and $(B^{4+}_{Me}{}^{3+})^{\bullet}$ (= holes localized at B^{3+} ions on the Me sublattice); Me = A and/or B. The oxygen activity dependence of the majority defect concentrations can also be obtained from the calculations performed; it is −1/6 at low a_{O_2}, i.e., $[(V_O{}^{2-})^{\bullet\bullet}] \propto [(B^{2+}_{Me}{}^{3+})'] \propto a_{O_2}^{-1/6}$, and 3/16 at high a_{O_2} where $[(V_{Me}{}^{3+})'''] \propto [(B^{4+}_{Me}{}^{3+})^{\bullet}] \propto a_{O_2}^{3/16}$.

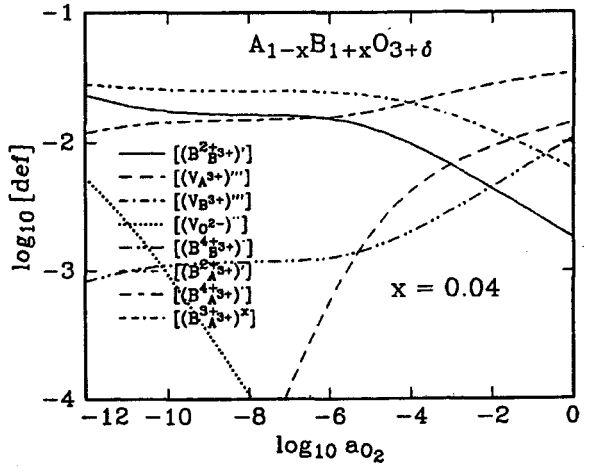

Fig. 31: Kröger-Vink diagram for $A_{1-x}B_{1+x}O_{3+\delta}$ with x = 0.04.

The deviation from stoichiometry, δ, can be calculated from the different vacancy concentrations by using the relation

$$\delta = \frac{3[(V_{La^{3+}})'''] + 3[(V_{Mn^{3+}})'''] - 2[(V_{O^{2-}})^{\bullet\bullet}]}{2 - 3[(V_{La^{3+}})'''] - 3[(V_{Mn^{3+}})''']} \qquad (17)$$

Values calculated for the deviation from stoichiometry, δ, for different cationic compositions by assuming the same set of equilibrium constants as used for generating the Kröger-Vink diagrams shown in Figs. 29-31 are plotted in Fig. 32. From the data shown in the plot one can determine the oxygen activity dependence of δ; $\delta \propto a_{O_2}^{-1/6}$ at low a_{O_2} and $\delta \propto a_{O_2}^{3/16}$ at high a_{O_2}. According to the curves shown in Fig. 32 the branches at high a_{O_2} are different for different x. At a given oxygen activity δ as a function of x has a minimum at x = 0; δ increases with increasing values of $|x|$.

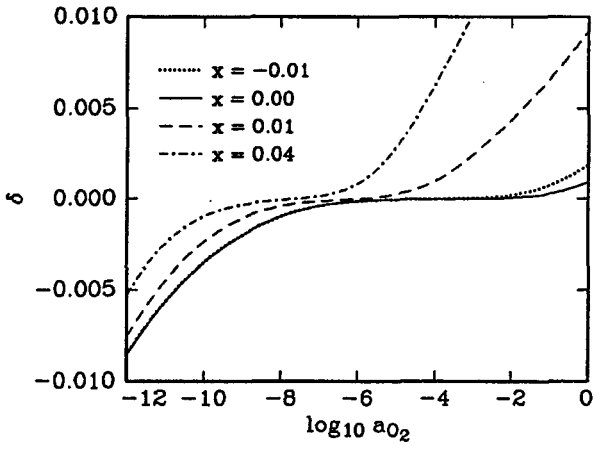

Fig. 32: δ as a function of x in $A_{1-x}B_{1+x}O_{3+\delta}$.

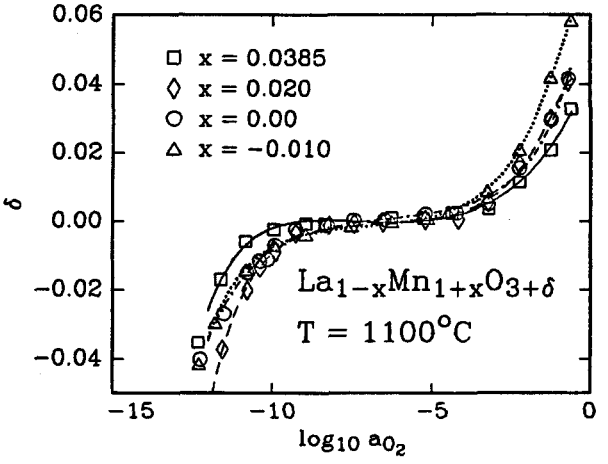

Fig. 33: Deviation from stoichiometry, δ, in $La_{1-x}Mn_{1+x}O_{3+\delta}$ with different x at 1100 °C as a function of log a_{O_2}.

We have also performed thermogravimetric measurements on the deviation from stoichiometry δ in $La_{1-x}Mn_{1+x}O_{3+\delta}$. Some results for δ are shown in Fig. 33. According to this figure, the largest deviations from stoichiometry observed (and with that the largest defect concentrations) are on the order of several percent. In general, with increasing point defect concentrations in ionic solids, the distance between the charged defects decreases and the electrostatic interaction between them increases. As a result, the mean activity coefficient of the charged defects decreases. At such high point defect concentrations as being present at very high and at very low oxygen activities in $La_{1-x}Mn_{1+x}O_{3+\delta}$, see Fig. 33, the Coulomb interaction between the charged defects cannot be ignored anymore (as done very often). The decrease of the mean activity coefficient, $f_{\pm}$, with increasing defect concentration leads to larger oxygen activity dependences than those expected for an ideal solution. The decrease leads to an upward bending of log [def] vs. log a_{O_2} at high defect concentrations. Values for the mean activity coefficient of point defects can be estimated by using the Debye-Hückel theory. The equation useful for this purpose is

$$\ln f_{\pm} = \frac{z_+ \cdot z_- \cdot e_o^2}{8 \cdot \pi \cdot \epsilon_r \cdot \epsilon_0 \cdot kT} \cdot \left[\frac{1}{a + \sqrt{\frac{\epsilon_r \cdot \epsilon_0 \cdot kT}{e_o^2 \cdot \sum_i (c_i \cdot z_i^2)}}} \right] \qquad (18)$$

where ϵ_0 is the absolute dielectric constant, ϵ_r the relative dielectric constant of $LaMnO_3$, a the shortest distance between two charged defects and z_i the charges of the defects.

The procedure used to relate values of δ with the oxygen activity a_{O_2} is discussed in the following. At low oxygen activities oxygen vacancies, $(V_O 2-)^{\bullet\bullet}$, and electrons, assumed to be localized in the form of $(Mn_{Me}^{2+}3+)'$ with Me = A and/or B are the majority defects.

At low a_{O_2}, where the cation vacancy concentrations are negligibly small, the oxygen vacancy concentration is related to the deviation from stoichiometry as follows:

$$[(V_{O^{2-}})^{\bullet\bullet}] \approx -\delta \tag{19}$$

By using point defect thermodynamics one can find for the activity of oxygen vacancies

$$a_{(V_{O^{2-}})^{\bullet\bullet}} = \left(\frac{3 \cdot K_O}{4}\right)^{1/3} \cdot a_{O_2}^{-1/6} = K_1 \cdot a_{O_2}^{-1/6} = f_\pm \cdot [(V_{O^{2-}})^{\bullet\bullet}] \tag{20}$$

K_O is an equilibrium constant and K_1 a proportionality factor. At high oxygen activities, cation vacancies, $(V_{Me^{3+}})'''$, and holes, here assumed to be localized in the form of $(Mn_{Me}^{4+3+})^{\bullet}$, are the majority defects. At high a_{O_2}, where the oxygen vacancy concentration is negligibly small, the cation vacancy concentration is

$$[(V_{La^{3+}})'''] + [(V_{Mn^{3+}})'''] \approx \frac{2 \cdot \delta}{3 + \delta} \tag{21}$$

For the mean activity of cation vacancies one can then write

$$a_{(V_{Me^{3+}})'''} = K_2 \cdot a_{O_2}^{3/16} = f_\pm \cdot \{[(V_{La^{3+}})'''] + [(V_{Mn^{3+}})'''] \} \tag{22}$$

where K_2 is a proportionality factor.

The equations discussed above have been fitted to data experimentally obtained for δ in $La_{1-x}Mn_{1+x}O_{3+\delta}$ in high and low oxygen activity ranges. The data and the fits obtained are shown in Figs. 34-37.

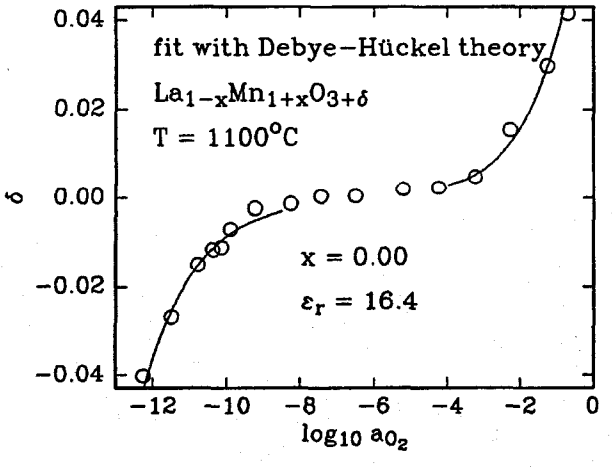

Fig. 34: δ in $La_{1-x}Mn_{1+x}O_{3+\delta}$ with x = 0 at 1100 °C as a function of log a_{O_2}. (Fits as described in the text.)

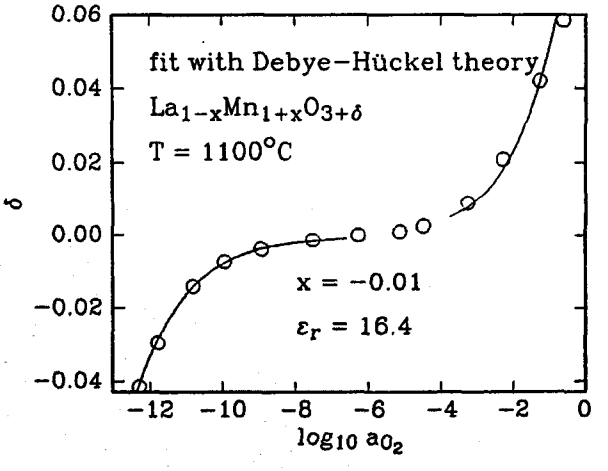

Fig. 35: δ in $La_{1-x}Mn_{1+x}O_{3+\delta}$ with x = − 0.01 at 1100 °C as a function of log a_{O_2}. (Fits as described in the text.)

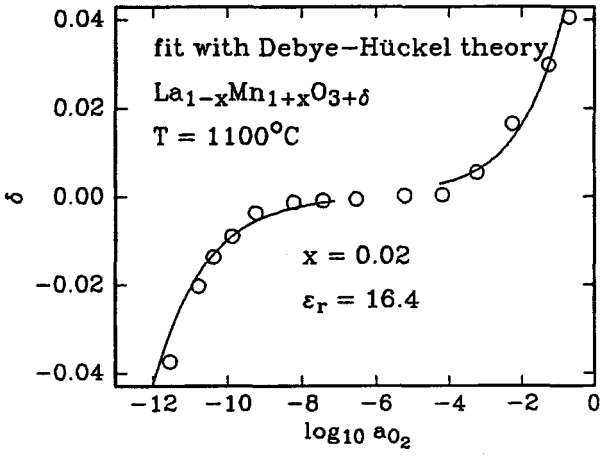

Fig. 36: δ in $La_{1-x}Mn_{1+x}O_{3+\delta}$ with x = 0.02 at 1100 °C as a function of log a_{O_2}. (Fits as described in the text.)

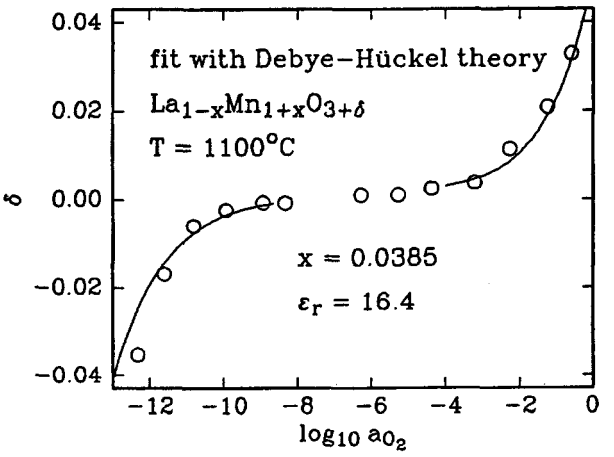

Fig. 37: δ in $La_{1-x}Mn_{1+x}O_{3+\delta}$ with x = 0.0385 at 1100 °C as a function of log a_{O_2}. (Fits as described in the text.)

In order to use the equation given earlier for estimating mean activity coefficients one needs to know the value of the relative dielectric constant of the material considered at the temperature of interest. Such data are rarely available. We have not found any value for ϵ_r of lanthanum manganite at high temperatures. However, we found a value for 80 K, i.e., ϵ_r = 20.5 [7]. In order to estimate a value for the relative dielectric constant at 1100 °C ϵ_r was initially used as a fitting parameter; the mean value obtained by fitting δ-values for different compositions x was then adopted and used for all subsequent fits. From the initial fits we obtained $\epsilon_r = 16.4 \pm 1.9$, i.e., a value not very far away from the value of 20.5 reported in the literature for 80 K [7]. From a second round of fitting (by using ϵ_r = 16.4) we obtained then values for the proportionality factors K_1 (related to formation of anion vacancies) and K_2 (related to the formation of cation vacancies. The values obtained for K_1 and K_2 at 1100 °C are displayed in Figs. 38 and 39, respectively. As one can see from these figures there are variations of K_1 and K_2 with the cationic composition which are not compatible with the assumption of a set of equilibrium constants which does not vary with the cationic composition x. Such an assumption was used to generate Figs. 29-32. The reasons behind are still unclear. The variations found for K_1 as a function of x at 1100, 1200 and 1300 °C are not very large and also do not show a common trend. The values obtained for K_2 slightly increase with increasing x and do not show any significant temperature dependence between 1100 and 1300 °C. More experimental data would be needed to establish the observed variations of K_1 and K_2 more precisely and then to possibly model these variations.

The electrical conduction of $LaMnO_3$ is reported to be by small polaron hopping [8,9], i.e., the electronic carriers are strongly localized, most likely at Mn^{3+} ions. Experimental data available from the literature [4,5] for the electrical conductivity, σ, do not show any

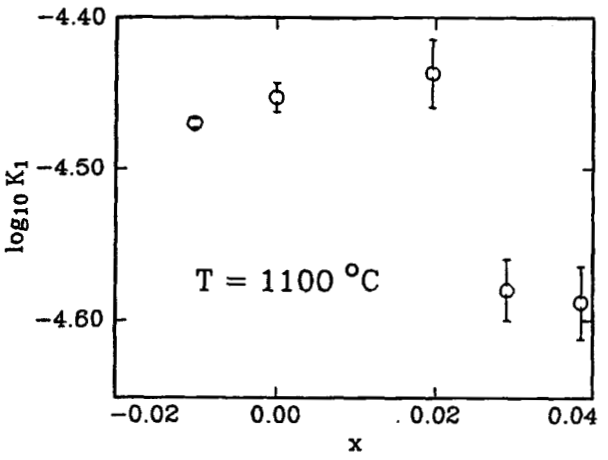

Fig. 38: Variation of the proportionality factor K_1 as a function of x in $La_{1-x}Mn_{1+x}O_{3+\delta}$ at 1100 °C.

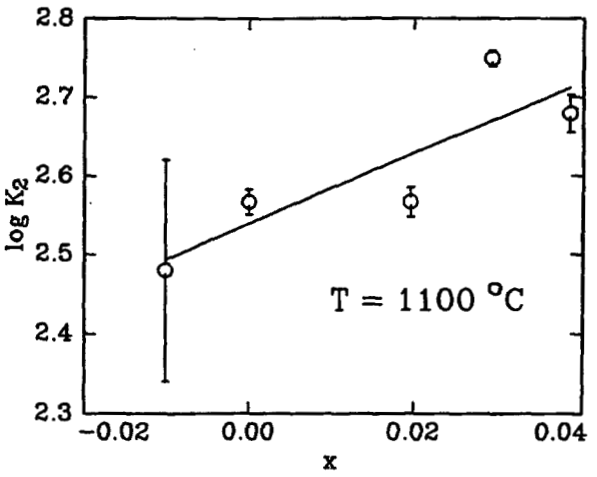

Fig. 39: Variation of the proportionality factor K_2 as a function of x in $La_{1-x}Mn_{1+x}O_{3+\delta}$ at 1100 °C.

visible contribution of electrons to the electronic conduction, suggesting that the conduction of holes is predominant. At high a_{O_2}, σ was observed to be approximately constant, see Fig. 28, although the overall hole concentration increases with increasing a_{O_2}, see the experimental values determined by us for δ at high a_{O_2}. As mentioned before, different explanations have been offered in the literature for the experimentally observed oxygen activity dependence of the electrical conductivity. However, all explanations known to us have some shortcomings.

One of the explanations offered in the literature [10] is that the majority defects at high oxygen activities are neutral associates consisting of holes and cation vacancies, $\{(V_{Me}3+)'''\cdot 3\,h^{\bullet}\}^{x}$. If such associates would be the majority defects in $La_{1-x}Mn_{1+x}O_{3+\delta}$, one would also not expect any changes in the electrical conductivity at high a_{O_2}. However, in this case one would expect that $\delta \propto a_{O_2}^{3/4}$, which is incompatible with the experimental results obtained for δ.

We offer an alternative explanation for the type of oxygen activity dependence observed for the electrical conductivity based on the presence of different types of holes with very different mobilities, i.e., some of the holes are considered to be trapped. A qualitative explanation of the oxygen activity dependence of the experimental results for σ shown in Fig. 28 is possible based on the following picture: i) most of the electrons present in $La_{1-x}Mn_{1+x}O_{3+\delta}$ are trapped at $(Mn^{3+}_{Mn}3+)^{x}$, ii) an insignificant fraction of the electrons is trapped at $(Mn^{3+}_{La}3+)^{x}$, iii) a fraction of the holes is trapped at $(Mn^{3+}_{Mn}3+)^{x}$, iv) a minor fraction of the holes is trapped at $(Mn^{3+}_{La}3+)^{x}$, and, to be compatible with the data for σ, v) there is hole hopping involving Mn^{4+} and Mn^{3+} ions on La^{3+} sites so that $\sigma \propto [(Mn^{4+}_{La}3+)^{\bullet}]\cdot[(Mn^{3+}_{La}3+)^{x}] \approx$ constant at high a_{O_2}, as one can conclude from the

results of a model calculation shown in Fig. 40 and based on the same equilibrium constant which were used to generate the Kröger-Vink diagram shown in Fig. 30.

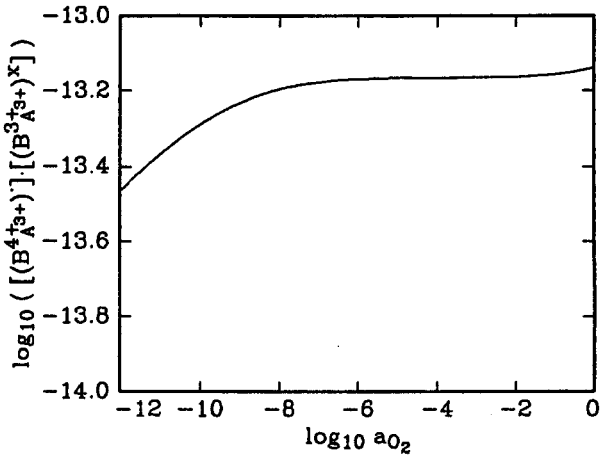

Fig. 40: Plot of $[(B^{4+}_{A^{3+}})^{\bullet}]\cdot[(B^{3+}_{A^{3+}})^{x}]$ ($\propto \sigma$) for $A_{1-x}B_{1+x}O_{3+\delta}$ with x = 0.

When thermodynamic variables such as the temperature and the oxygen activity are changed, the composition of $La_{1-x}Mn_{1+x}O_{3+\delta}$ changes to that corresponding to the equilibrium state for the new thermodynamics variables. In general, the relaxation rate is determined by the rate of the processes taking place at the gas/solid interface and by mass transport within the oxide, i.e., chemical diffusion. Parameters used to characterize the rate of the surface reaction and of the chemical diffusion are phenomenological surface reaction constant, k, and a chemical diffusion coefficient, $\tilde{D}$. The value of the surface reaction constant is very important for the performance of solid oxide fuel cells. If this value is small for an electrode material due to a slow surface reaction, electrode polarization occurs which reduces the cell performance.

Initially as a by-product of our measurements of changes in the oxygen content, we have followed the kinetics of compositional changes in $La_{1-x}Mn_{1+x}O_{3+\delta}$ as a function of the time after oxygen activity jumps. We have consistently observed that the kinetics of oxygen content changes upon jumps between two given oxygen activity changes depend on the jump direction, see Figs. 41-43. The samples used in the measurements performed for Figs. 41-43 were thin, round discs. The results shown in Figs. 41-43 allow to conclude that the relaxation rate is always larger in reducing than in oxidizing direction. Furthermore, one can also conclude without any doubts from Figs. 41 and 42 that the relaxation rate increases significantly with increasing oxygen activity at a given cationic composition x when CO/CO_2 gas mixtures are present. Preliminary results obtained by using samples with poorly defined geometries showed that there is a very significant change in the relaxation rate with the cationic composition for a given oxygen activity jump. The reaction rate increases very significantly when the La content increases.

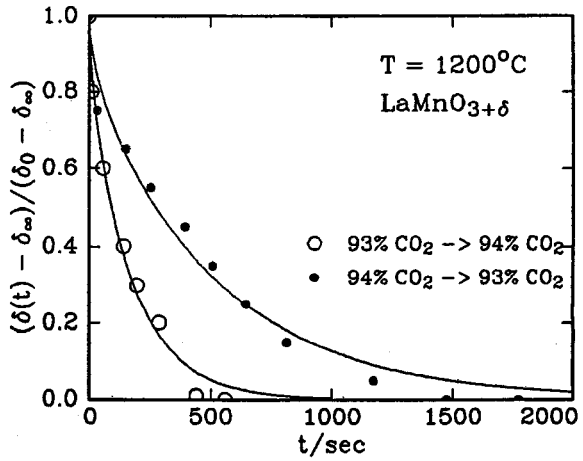

Fig. 41: Relative change in δ observed upon oxygen activity changes at relatively low a_{O_2} in $La_{1-x}Mn_{1+x}O_{3-\delta}$ with x = 0 at 1200 °C. P = 0.55 atm.

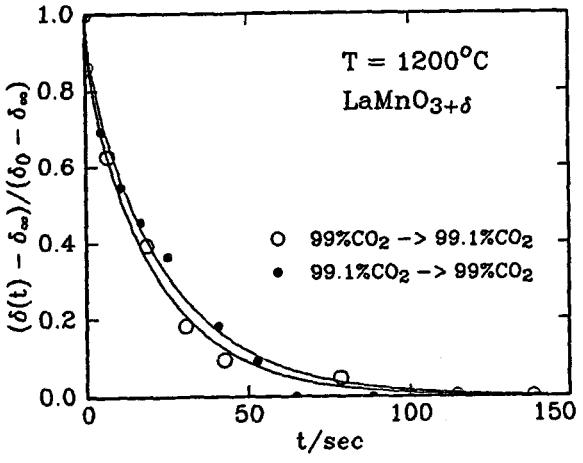

Fig. 42: Relative change in δ observed upon oxygen activity changes at intermediate a_{O_2} in $La_{1-x}Mn_{1+x}O_{3-\delta}$ with x = 0 at 1200 °C. P = 0.55 atm.

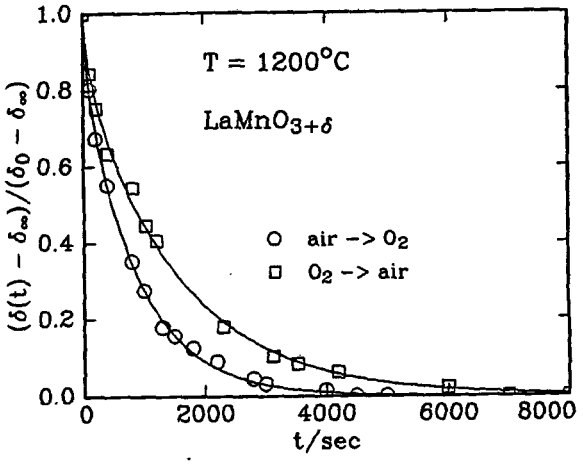

Fig. 43: Relative change in δ observed upon oxygen activity changes at high a_{O_2} in $La_{1-x}Mn_{1+x}O_{3-\delta}$ with x = 0 at 1200 °C. P = 0.55 atm.

From the experimental data shown in Figs. 41-43 and additional, similar data we have determined values for the chemical diffusion coefficient and for the phenomenological rate constant involved in the compositional changes after oxygen activity jumps. The data obtained are shown in Figs. 44 and 45. As one can see from these figures there is a

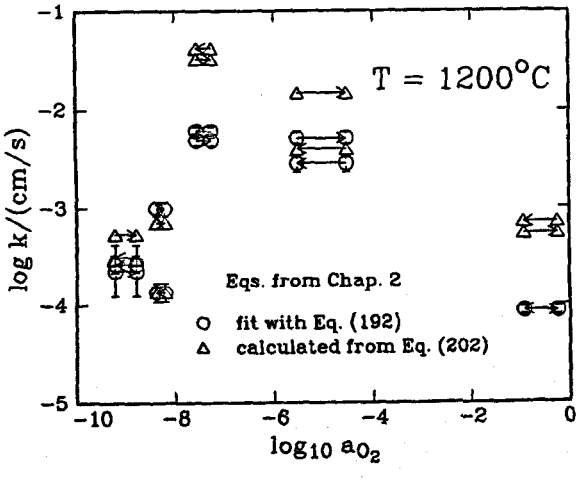

Fig. 44: Oxygen activity dependence of the phenomenological surface reaction constant, k, for $LaMnO_{3+\delta}$ at 1200 °C.

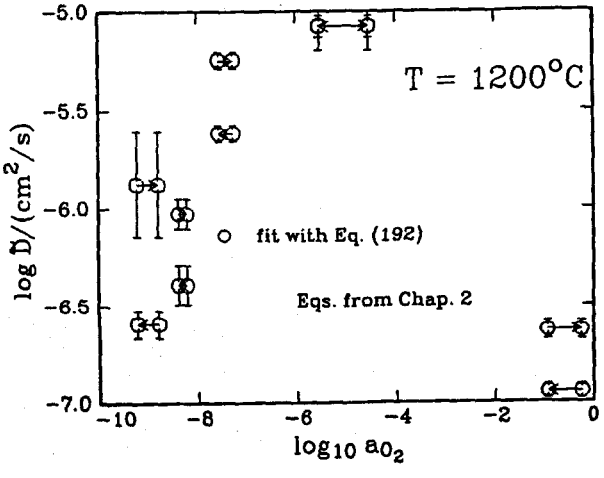

Fig. 45: Oxygen activity dependence of the chemical diffusion coefficient, $\tilde{D}$, in $LaMnO_{3+\delta}$ at 1200 °C.

strong oxygen activity dependence for both, the chemical diffusion coefficient and the phenomenological rate constant. Knowledge of such oxygen activity dependences is of great interest for applications like SOFC cathodes. Therefore, it is intended to continue to perform the type of relaxation measurement just described in a new research program and to extend them to doped $LaMnO_3$ and other potential cathode materials for SOFC materials.

References

[1] F.-H. Lu, S. Tinkler, and R. Dieckmann, "Point Defects and Cation Tracer Diffusion in $(Co_xFe_{1-x})_{3-\delta}O_4$ Spinels," Solid State Ionics, **62** (1-2) [1993] 39-52.

[2] J.A.M. van Roosmalen, P. van Vlaaderen, E.H.P. Cordfunke, W.L. Ijdo and D.J.W. Ijdo, "Phases in the Perovskite $LaMnO_{3+\delta}$ Solid Solution and the La_2O_3-Mn_2O_3 Phase Diagram," J. Solid State Chem., **114** [1995] 516-523.

[3] J.H. Kuo, H.U. Anderson, and D.M. Sparlin, "Oxidation-Reduction Behavior of Undoped and Sr-doped $LaMnO_3$ Nonstoichiometry and Defect Structure," J. Solid State Chem., **83** [1989] 52-60.

[4] J. Mizusaki, H. Tagawa, Y. Yonemura, H. Minamiue, and H. Nambu, "Effect of Lanthanum Deficiency on the Nonstoichiometry Electronic Properties and Structure of $La_{1-x}MnO_{3+\delta}$," in: 'Proc. 2nd International Symposium on Ionic and Mixed Conducting Ceramics,' San Francisco, CA, T.A. Ramaranyanan, W.L. Worrell and H.L. Tuller, Eds., Electrochem. Soc. Proc., **94-12** [1994] 402-411.

[5] J.H. Kuo, H.U. Anderson, and D.M. Sparlin, "Oxidation-Reduction Behavior of Undoped and Sr-doped $LaMnO_3$: Defect Structure, Electrical Conductivity and Thermoelectric Power," J. Solid State Chem., **87** [1990] 55-63.

[6] J. Töpfer and R. Dieckmann (unpublished)

[7] V.Y. Ivanov, V.D. Travkin, A.A. Mukhin, S.P. Lededev, A.A. Volkov, A. Pimenov, A. Loidl, A.M. Balbashov, and A.V. Mozhaev, "Magnetic, Dielectric, and Transport Properties of $La_{1-x}Sr_xMnO_{3+\delta}$ at Submilimeter Wavelengths," J. Appl. Phys., **11** [1998] 7180-7182.

[8] R. Raffaelle, H.U. Anderson, D.M. Sparlin, and P.E. Parris, "Transport Anomalies in the High-Temperature Hopping Conductivity and Thermopower of Sr-doped $La(Cr,Mn)O_3$," Phys. Rev., **43** [1991] 7991-7999.

[9] L. Ranno, M. Viret, A. Mari, R.M. Thomas and J.M.D. Coey, "Stoichiometry and Electronic Properties of $LaMnO_3$," J. Phys., **8** [1996] L33-L36.

[10] J. Nowotny and M. Rekas, "Defect Chemistry of $(La,Sr)MnO_3$," J. Am. Ceram. Soc., **81** [1998] 67-80.

5. PUBLICATIONS

5.1. Recent Publications from this Project

Since the last report, no papers from this project were published. The following manuscripts from this project have been submitted for publication and need still small revisions in order to be published:

[1] **"Point Defects and Cation Tracer Diffusion in $(Ti_xFe_{1-x})_{3-\delta}O_4$: I. Nonstoichiometry and Point Defects"**
S. Aggarwal and R. Dieckmann
Phys. Chem. Miner.

[2] **"Point Defects and Cation Tracer Diffusion in $(Ti_xFe_{1-x})_{3-\delta}O_4$: II. Cation Tracer Diffusion"**
S. Aggarwal and R. Dieckmann
Phys. Chem. Miner.

[3] **"Contributions of Bulk and Near-Boundary Regions to the Variation of the Oxygen Content in $Cu_{2-\delta}O$"**
S. Aggarwal and R. Dieckmann
J. Phys. Chem. Solids

The following manuscripts from this project are close to be submitted for publication:

[1] **"Defects and Transport in Cobaltous Oxide, $Co_{1-\Delta}O$: I. Experimental Study of the Variation of Stoichiometry, Electrical Conductivity and Thermopower with Oxygen Activity"**
S. Aggarwal, F. Morin and R. Dieckmann

[2] **"Defects and Transport in Cobaltous Oxide, $Co_{1-\Delta}O$: II. Relationships Between Deviation From Stoichiometry, Cation Tracer Diffusion, Electrical Conduction and Thermopower"**
S. Aggarwal and R. Dieckmann

[3] **"Does the Valence State of an Ion Affect its Diffusivity?"**
E. Chen, T.-L. Tsai and R. Dieckmann

[4] **Does the Valence State of an Ion Affect its Diffusivity in a Spinel Structure?"**
Y.H. Ha and R. Dieckmann

5.2. Other Publications

Other manuscripts published or accepted after the last report:

[1] **"Sodium Tracer Diffusion in an Alkaline-Earth Boroaluminosilicate Glass"**
L. Tian and R. Dieckmann
J. Non-Cryst. Solids, **265** [2000] 36-40.

[2] **"Influence of 'Water' on the Diffusion of Sodium in Fused Quartz and in an Alkaline-Earth Aluminoborosilicate Glass"**
L. Tian, R. Dieckmann, Y.-Y. Lin and C.-Y. Hui, Proceedings CIMTEC International Conference on 'Mass Transport in Inorganic Materials - Fundamentals to Devices,' May 28 - June 2, 2000, Venice, Italy. (submitted March 22, 2000, accepted)

[3] **"Bulk Diffusion Measurements to Study the Effectiveness of Barrier Layers"**
L. Tian, R. Dieckmann, Y.-Y. Lin and C.-Y. Hui, Proceedings CIMTEC International Conference on 'Mass Transport in Inorganic Materials - Fundamentals to Devices,' May 28 - June 2, 2000, Venice, Italy. (submitted March 22, 2000, accepted)

[4] **"Sodium Tracer Diffusion in a Glass-Ceramic Containing Nano-Sized Spinel Crystals"**
L. Tian and R. Dieckmann
J. Non-Cryst. Solids, **281** (1-3) [2001] 55-60.

[5] **"Effect of Water Incorporation on the Diffusion of Sodium in an Alkaline-Earth Boroaluminosilicate Glass"**
L. Tian, R. Dieckmann, C.-Y. Hui and J.G. Couillard
J. Non-Cryst. Solids, **296** (1-2) [2001] 123-134.

[6] **"Effect of Water Incorporation on the Diffusion of Sodium in in Type I Silica Glass"**
L. Tian, R. Dieckmann, C.-Y. Hui, Y.-Y. Lin and J.G. Couillard
J. Non-Cryst. Solids, **286** (3) [2001] 146-161.

[7] **"Impurity Controlled Phase Formation at Platinum-Sapphire Interfaces"**
M.J. Murtagh, J. Hulvat, R. Dieckmann and S.L. Sass
Acta metall. mater., **49** (17) [2001] 3493-3504.

[8] **"Bulk Diffusion Measurements to Study the Effectiveness of Barrier Layers: I. Mathematical Treatment"**
L. Tian, M.O. Thompson, R. Dieckmann, C.-Y. Hui and Y.-Y. Lin
J. Appl. Phys., **90** (8) [2001] 3799-3809.

[9] **"Bulk Diffusion Measurements to Study the Effectiveness of Barrier Layers: II. Exchange of Sodium Between Liquid Crystal Display Glass Substrates with Different Barrier Layers"**
L. Tian and R. Dieckmann
J. Appl. Phys., **90** (8) [2001] 3810-3815.

Other manuscripts which were submitted and still need to be revised are:

[1] **"Variation of the Oxygen Content and Point Defects in Olivines, $(Fe_xMg_{1-x})_2SiO_{4+\delta}$, $0.2 \leq x \leq 1.0$"**
T.-L. Tsai and R. Dieckmann
Phys. Chem. Miner.

[2] **"Deviation from Stoichiometry and Point Defects in Tephroite, $Mn_2SiO_{4+\delta}$"**
J. Töpfer and R. Dieckmann
Phys. Chem. Miner.

6. PRESENTATIONS

Between April 16, 1999, and December 12, 2001, there were 14 project-related presentations:

"Influence of the Grain Size on the Oxygen Content and the Cation Tracer Diffusion in Polycrystalline Magnetite, $Fe_{3-\delta}O_4$"
S. Desai and R. Dieckmann
101st Annual Meeting American Ceramic Society, April 25 - 28, 1999, Indianapolis, Indiana, U.S.A. (talk).

"Point Defect Chemistry of Perovskites, $A_{1-\xi}B_{1+\xi}O_{3+\delta}$"
H. Oh and R. Dieckmann
101st Annual Meeting American Ceramic Society, April 25 - 28, 1999, Indianapolis, Indiana, U.S.A. (talk).

"Oxygen Activity Dependence of the Tracer Diffusion of Impurity Transition Metal Cations in Doped Oxides"
C. Stanek and R. Dieckmann
101st Annual Meeting American Ceramic Society, April 25 - 28, 1999, Indianapolis, Indiana, U.S.A. (talk).

"Point Defects and Cation Tracer Diffusion in $(Ni_xFe_{1-x})_{3-\delta}O_4$"
L. Liu and R. Dieckmann
101st Annual Meeting American Ceramic Society, April 25 - 28, 1999, Indianapolis, Indiana, U.S.A. (talk).

"Point Defects and Transport in Non-Stoichiometric Oxides and Cation Diffusion in Glasses"
R. Dieckmann
Seminar, Materials Science and Engineering Department, Rensselaer Polytechnic Institute, April 20, 2000, Troy, NY, U.S.A.

"Variation of the Oxygen Content in Perovskites of the Type $La_{1-\xi}Mn_{1+\xi}O_{3+\delta}$"
H. Oh and R. Dieckmann
102nd Annual Meeting American Ceramic Society, April 30 - May 3, 2000, St. Louis, Missouri, U.S.A. (talk).

"Point Defects, Deviation from Stoichiometry and Cation Tracer Diffusion in $(Ni_xFe_{1-x})_{3-\delta}O_4$"
L. Liu and R. Dieckmann
102nd Annual Meeting American Ceramic Society, April 30 - May 3, 2000, St. Louis, Missouri, U.S.A. (talk).

"Influence of the Oxygen Activity on Point Defects and on Transport in Non-Stoichiometric Oxides"
R. Dieckmann
Seminar, National Institute for Research in Inorganic Materials (NIRIM), Tsukuba, Japan, October 17, 2000

"Ceramic Science - a wide field: some News on Point Defects in Non-Stoichiometric Oxides and on the Diffusion of Sodium in Oxide Glasses"
R. Dieckmann
Seminar, Department of Materials Science, Japan Atomic Energy Research Institute, Tokai, Japan (JAERI), October 24, 2000.

"Point Defects and Transport in Non-Stoichiometric Oxides and Cation Diffusion in Glasses"
R. Dieckmann
Seminar (Materials Research Lecture Series), California Institute of Technology, November 15, 2000.

"Point Defects in Perovskites of the Type $A_{1-x}B_{1+x}O_{3+\delta}$ with Localized Electronic Defects"
H. Oh and R. Dieckmann
103rd Annual Meeting American Ceramic Society, April 22 - 25, 2001, Indianapolis, Indiana, U.S.A. (poster).

"Influence of the Charge State of Cations on Their Diffusivity in Oxides and in Silica Glass"
R. Dieckmann, E. Chen, Y.H. Ha, Y.H. Lau, W. Chang, C. Stanek, and L. Tian
103rd Annual Meeting American Ceramic Society, April 22 - 25, 2001, Indianapolis, Indiana, U.S.A. (talk).

"Point Defects and Transport of Matter and Charge in Oxides at High Temperatures and Solid State Reactions"
R. Dieckmann
Workshop on Materials for Fuel Cells, National Fuel Cell Research Center (NFCRC), Irvine, CA, August 7-8, 2001 (talk).

"Influence of the Charge State of Cations on Their Diffusivity in Crystalline Oxides and in Silica Glass"
R. Dieckmann, E. Chen, Y.H. Ha, Y.H. Lau, W. Chang, C. Stanek, and L. Tian
United Engineering Foundation (UEF) Conference "Nonstoichiometric Ceramics and Intermetallics," Barga, Italy, September 30 - October 5, 2001 (talk).

Other presentations:

"Influence of 'Water' on the Diffusion of Sodium in Corning Code 1737 Glass"
L. Tian and R. Dieckmann
101st Annual Meeting American Ceramic Society, April 25 - 28, 1999, Indianapolis, Indiana, U.S.A. (talk).

"Bulk Diffusion Measurements to Study the Effectiveness of Barrier Layers"
L. Tian and R. Dieckmann
101st Annual Meeting American Ceramic Society, April 25 - 28, 1999, Indianapolis, Indiana, U.S.A. (talk).

"Influence of the Surrounding Atmosphere on the Diffusion of Sodium in an Alkaline-Earth Boroaluminosilicate Glass (Corning Code 1737)"
L. Tian and R. Dieckmann
102nd Annual Meeting American Ceramic Society, April 30 - May 3, 2000, St. Louis, Missouri, U.S.A. (talk).

"Formation of Nickel Oxide (NiO) by Oxidation of Ni_xPt_{1-x} Alloys"
R. Pornprasertsuk and R. Dieckmann
102nd Annual Meeting American Ceramic Society, April 30 - May 3, 2000, St. Louis, Missouri, U.S.A. (poster).

"Influence of 'Water' on the Diffusion of Sodium in Fused Quartz Glass"
L. Tian and R. Dieckmann
102nd Annual Meeting American Ceramic Society, April 30 - May 3, 2000, St. Louis, Missouri, U.S.A. (talk).

"Oxygen Activity Dependence of the Diffusion of Iron and Cobalt in SiO_2 Glass"
L. Tian and R. Dieckmann
102nd Annual Meeting American Ceramic Society, April 30 - May 3, 2000, St. Louis, Missouri, U.S.A. (talk).

"Influence of 'Water' on the Diffusion of Sodium in Fused Quartz and in an Alkaline-Earth Aluminoborosilicate Glass"
L. Tian, R. Dieckmann, Y.-Y. Lin and C.-Y. Hui
CIMTEC International Conference on 'Mass Transport in Inorganic Materials - Fundamentals to Devices,' May 28 - June 2, 2000, Venice, Italy (talk).

"Bulk Diffusion Measurements to Study the Effectiveness of Barrier Layers"
L. Tian, R. Dieckmann, Y.-Y. Lin and C.-Y. Hui
CIMTEC International Conference on 'Mass Transport in Inorganic Materials - Fundamentals to Devices,' May 28 - June 2, 2000, Venice, Italy (poster).

"Influence of 'Water' on the Diffusion of Sodium in Corning Code 1737 Glass"
L. Tian, R. Dieckmann and C.-Y. Hui
Glass & Optical Materials Division Meeting (American Ceramic Society), October 1-4, 2000, Corning, New York, U.S.A. (talk).

"Influence of 'Water' on the Diffusion of Sodium in Fused Quartz Glass"
L. Tian, R. Dieckmann, Y.-Y. Lin and C.-Y. Hui
Glass & Optical Materials Division Meeting (American Ceramic Society), October 1-4, 2000, Corning, New York, U.S.A. (talk).

"Sodium Tracer Diffusion in $(CaO \cdot Al_2O_3)_{1-x}(SiO_2)_x$ Glasses"
R. Pornprasertsuk and R. Dieckmann
103rd Annual Meeting American Ceramic Society, April 22 - 25, 2001, Indianapolis, Indiana, U.S.A. (talk).